Letter | Editors' Suggestion

Stabilization of collinear ferromagnetic order in Ir-doped triple-layer ruthenate $Sr_4Ru_3O_{10}$

Feng Ye,[1,*] Zachary Morgan,[1] Yu Zhang,[2] Yifei Ni,[2] and G. Cao[2]

[1]*Neutron Scattering Division, Oak Ridge National Laboratory, Oak Ridge, Tennessee 37831, USA*

[2]*Department of Physics, University of Colorado at Boulder, Boulder, Colorado 80309, USA*

(Received 13 September 2023; revised 10 November 2023; accepted 30 November 2023; published 14 December 2023)

The triple-layer $Sr_4Ru_3O_{10}$ is a spin-orbit-coupled metal featuring an intriguing combination of ferromagnetic and metamagnetic states. Here we report a comprehensive study of single-crystal neutron and x-ray diffraction on $Sr_4Ru_3O_{10}$ with 4% iridium doping. The system crystallizes in an orthorhombic *Bbem* structure in which two triple layers are related by a base centering symmetry operation within one unit cell. The 4% Ir doping at the Ru site sensitively alters the structural balance between the RuO_6 layers, as such the two outer-layer octahedra rotate 6.7° about the *c* axis, while the central-layer one rotates in the opposite direction by 11.0°. The increased lattice distortion stabilizes a collinear ferromagnetic state with magnetic moments fully aligned along the *c* axis. The emerging perpendicular magnetic anisotropy naturally increases the critical field for the inplane metamagnetic transition to 4.5 Tesla. All results highlight the critical linkage between the magnetic properties and underlying lattice through orbital degrees of freedom, as well as the enhanced spin orbit coupling due to heavier 5*d* ions. Our observation provides a viable route for an efficient manipulation of the magnetic states with functionalities.

DOI: 10.1103/PhysRevB.108.L241109

The strontium ruthenate of the Ruddlesden-Popper (RP) series, $Sr_{n+1}Ru_nO_{3n+1}$, plays a pivotal role in studying strongly correlated electron systems with significant spin-orbit interactions (∼0.16 eV for Ru^{4+}). They exhibit a rich array of physical properties including unconventional superconductivity in single-layer ($n = 1$) Sr_2RuO_4 [1–4], magnetic-field tuned quantum criticality in bilayer ($n = 2$) $Sr_3Ru_2O_7$ [5,6], and isotropic itinerant ferromagnetism in $SrRuO_3$ ($n = \infty$) [7,8] that is widely used as a conductive layer in epitaxial films or heterostructure/superlattices for a variety of functional oxides [9]. A common feature in this class of materials is the small energy variance between different crystal structures and magnetic states due to the complex interplay between spin, orbital, and lattice degrees of freedom. As such, the ground state is close to an instability and prone to change drastically due to small external perturbations [10,11].

The quasi-two-dimensional triple-layer $Sr_4Ru_3O_{10}$ shows both a prominent *c*-axis ferromagnetic (FM) state and an inplane metamagnetic state, a behavior both intriguing and puzzling [12]. The spin configuration and the nature of the metamagnetic transition have remained controversial despite intensive investigations of the ruthenate since its first report. It was initially proposed that the Ru ions possess canted moments, with spins oriented primarily along the *c* axis and tilted toward the basal plane below $T_C \approx 105$ K [12–14]. The tilting amplitude reaches its maximum at $T^* \approx 60$ K and is suppressed at low temperature. An earlier study suggested that a strong magnetocrystalline anisotropy locks the spins in the basal plane with no sign of antiferromagnetic (AFM) correlation [15]. A more recent work revealed that the magnetic structure has moments only aligning along the *c* axis [16]. Recent neutron diffraction experiments indicated that the $Sr_4Ru_3O_{10}$ carries an extra inplane component in the intermediate temperature range around T^* [17,18]. Detailed analysis indicates that the Ru moments of the central layer RuO_6 octahedra are aligned along the *c* axis while those of the two outer layers lie in the basal plane with an antiferromagnetic configuration, thus forming a layer-dependent antiferromagnetism near T^* [18]. These reports clearly indicate that the magnetic state of $Sr_4Ru_3O_{10}$ is near an instability, and can be readily tuned, for example, using chemical substitution or hydrostatic pressure [10,19]. In this Letter, we report a comprehensive neutron and x-ray diffraction study of the crystal and magnetic structures of Ir-doped $Sr_4Ru_3O_{10}$. A small amount of iridium at the Ru site (∼4%) alters the rotations of RuO_6 octahedra of the triple-layers [Fig. 1(a)]. As a result, it suppresses the antiferromagnetic correlation in the pristine $Sr_4Ru_3O_{10}$, and stabilizes a robust, collinear ferromagnetic spin order. The enhanced perpendicular magnetic anisotropy renders a significantly higher critical field of 4.5 T for the occurrence of the basal-plane metamagnetic state.

Single crystals of Ir-doped $Sr_4Ru_3O_{10}$ were grown using a self-flux method from off-stoichiometric quantities of RuO_2, $SrCO_3$, and $SrCl_2$. Magnetic properties were measured using a quantum design MPMS-7 superconducting quantum interference device magnetometer. The structure information of the crystal was investigated using a Rigaku XtaLAB PRO diffractometer equipped with a HyPix-6000HE detector on single crystals with a dimension of $0.1 \times 0.1 \times 0.01$ mm^3. A molybdenum anode was used to generate x-rays with wavelength $\lambda = 0.7107$ Å. The samples were cooled by cold nitrogen flow provided by an Oxford N-Helix cryosystem. A single crystal with a size approximately $1.5 \times 1.5 \times 0.5$ mm^3 was chosen for the diffraction study using the CORELLI diffractometer [20] at the Spallation Neutron Source of Oak Ridge

*yef1@ornl.gov

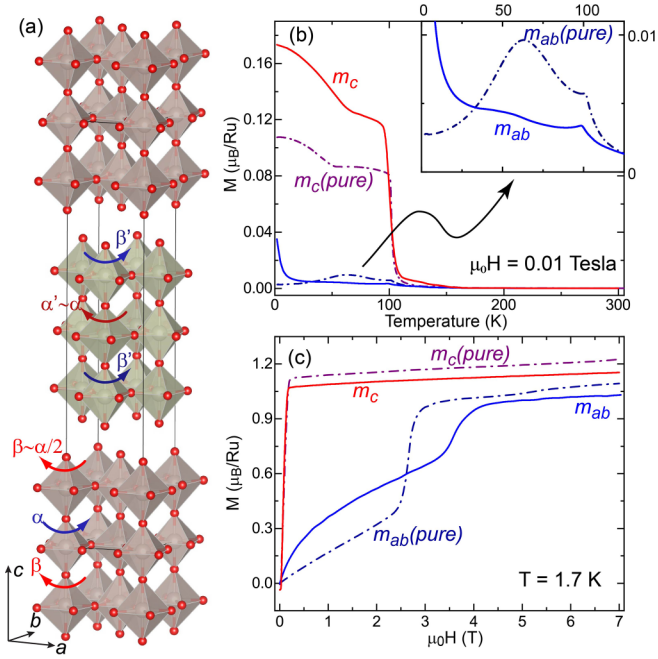

FIG. 1. (a) The crystal structure of $Sr_4(Ru_{1-x}Ir_x)_3O_{10}$ and schematics of the RuO_6 octahedra rotations. The octahedra of central layer rotate along the c axis by α and α', while the outer-layer octahedra rotate in the opposite direction by β and β', respectively. (b) Comparison of the magnetization for pure (dashed lines) and Ir-doped (solid lines) $Sr_4Ru_3O_{10}$ as function of temperature for magnetic field in the basal plane and along the c axis at $\mu_0 H = 0.01$ T. Inset shows the region for m_{ab} from 5 K to 150 K. (c) Comparison of the isothermal magnetization with respect to the magnetic field at 1.7 K for the pure and Ir-doped $Sr_4Ru_3O_{10}$.

National Laboratory. The sample was aligned in both the $[h, 0, l]$ and $[h, h, l]$ scattering planes for the zero-field study using a closed cycle refrigerator, and subsequently placed in a 5 T superconducting magnet to study the field-dependent evolution of the spin configuration.

Figure 1(b) compares the c axis and in-plane magnetization M_c and M_{ab} of the undoped and Ir-doped $Sr_4Ru_3O_{10}$ single crystals. Both show a magnetic transition at 105 K identified by the abrupt increase in M_c and considerable anisotropy between M_c and M_{ab}. A large c-axis magnetization signifies the moment is predominantly along that direction. However, the sharp transition at T^* is suppressed more in the doped crystal, compared to that in the undoped one [inset of Fig. 1(b)]. Consistently, the metamagnetic transition rises to 4.5 T from 2.5 T for the doped and undoped samples, respectively. All indicate a significant change in the spin configuration in the Ir-doped $Sr_4Ru_3O_{10}$.

One major characteristic of the layered ruthenates is that the electronic and magnetic properties are critically linked to the underlying lattice through orbital degrees of freedom [21–23]. We therefore first investigate whether the modification of magnetic properties is reflected in the lattice distortion. In undoped $Sr_4Ru_3O_{10}$, the building block consists of triple-layers of corner-sharing RuO_6 octahedra that show correlated counterrotations about the c axis [Fig. 1(a)]. The RuO_6 octahedra of two outer layers rotate by an average of $\beta \sim 5.6°$ in the same direction while the octahedra of the central layers rotated in the opposite direction by $\alpha \sim 11°$ [12]. An earlier study proposed that the $Sr_4Ru_3O_{10}$ crystallizes in a primitive orthorhombic structure (Space Group 55, *Pbam*). The neighboring Ru_3O_9 triple layers along the c axis are not related by symmetry and can have independent rotation angles of α' and β', respectively. The authors of Ref. [12] also considered space group *Bbem* as a possible structure where the RuO_6 in the triple-layer stacking are related by the B-centering symmetry operation and maintain the same rotation angles. Although a smaller refined R value led to the argument that the *Pbam* structure better describes the neutron powder diffraction pattern, the authors pointed out that a conclusive determination separating the subtle difference between the two choices should be conducted via high-quality single crystal neutron diffraction.

The structural characterization to elucidate the role of iridium substitution in $Sr_4(Ru_{1-x}Ir_x)_3O_{10}$ is conducted using single crystal neutron and x-ray diffraction. The crystal has an orthorhombic structure with lattice parameters of $a = 5.5052(2)$ Å, $b = 5.5062(2)$ Å, and $c = 28.592(1)$ Å at 250 K. The feature differentiating the *Pbam* from *Bbem* structure are nonzero (h, k, l) nuclear peaks with reflection condition $h + l = 2n + 1$. There is no appreciable intensity at the mentioned reflections, surveying a large area in different scattering planes. Details are given in the Supplemental Material [24]. This highlights that the *Bbem* is the proper space group. The stacked triple layers within the unit cell are equivalent and are thus constrained to have the same rotation angles, i.e., $\alpha' = \alpha$ and $\beta' = \beta$, for the corresponding octahedra. The structure factor of the $(2n, 1, l)$ peaks is contributed only by the oxygen positions of the RuO_6 octahedra. The intensity can be derived as

$$F^2 = 16[A_1 + 2A_2 \cos(2\pi z l)]^2, \tag{1}$$

where A_i is related to the in-plane rotation part $\cos[\pi(\cos\theta_i + 1/2 \sin\theta_i)] \cos[\pi(\sin\theta_i - 1/2 \cos\theta_i)]$ with $\theta_1 = \alpha, \theta_2 = -\beta$, and the $\cos(2\pi z l)$ term arises from the phase factor of the triple layer, $z \approx 0.14$ is the Wyckoff coordinate of the outer layer Ru ions. Figure 2 shows the neutron diffraction pattern in the $(h, 1, l)$ scattering plane collected at 150 K (above T_C). The intensity of Bragg reflections along the $[0, 0, l]$ direction across $(\pm 2, 1, 0)$ and $(\pm 4, 1, 0)$ peaks show periodic modulation and substantial intensities [red and blue curves in Figs. 2(b) and 2(c)]. They are comparable to neighboring nuclear peaks with contributions dominated by heavier Sr and Ru elements. Modeling the oxygen displacement using Eq. (1) with minimal parameters of the rotation angles α and β perfectly reproduces the modulated intensities. Full refinement reveals that the rotation angles of two outer-layer RuO_6 octahedra increase to 6.7° in the Ir-doped $Sr_4Ru_3O_{10}$, whereas the central-layer RuO_6 octahedron remains at 11.0°. In addition, both neutron and x-ray studies reveal that 4% Ir ions are randomly distributed at the two outer Ru sites with the central-layer Ru site only slightly iridium rich. A 0.5% reduction for the in-plane lattice parameters is consistent with the increased buckling of RuO_6 octahedra.

The enhanced lattice distortion has a consequential effect on the spin structure. The undoped $Sr_4Ru_3O_{10}$ borders between paramagnetic $Sr_3Ru_2O_7$ with ferromagnetic fluctuations

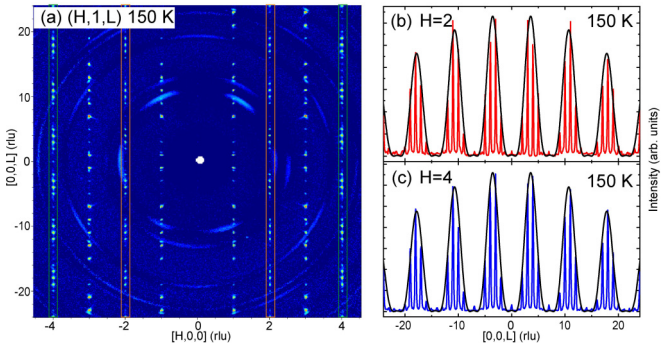

FIG. 2. (a) The neutron diffraction contour plot of $Sr_4Ru_{2.88}Ir_{0.12}O_{10}$ in the $(h, 1, l)$ scattering plane at 150 K (above the magnetic transition). The data were collected with the sample stick rotating 360 degrees about the vertical axis at three degrees step. The background is removed by subtracting the rotation-angle-independent median counts across all sample orientations for individual detector pixels. The weak ringlike feature originates from the coherent scattering background of the aluminum plate on which the single crystal was mounted. (b) The line cut along the $[0, 0, l]$ direction across the (2,1,0) Bragg peak. (c) Similar line cut along the $[0, 0, l]$ direction across the (4,1,0) peak. Black solid lines are the fitted envelopes using Eq. (1).

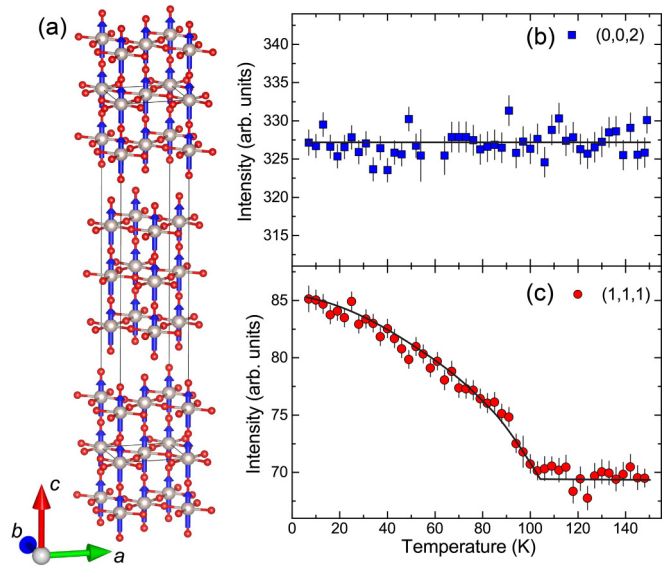

FIG. 3. The refined magnetic structure of $Sr_4Ru_{2.88}Ir_{0.12}O_{10}$ at $\mu_0 H = 0$. The Ru spins form a collinear FM configuration with moments along the c axis. (b) The temperature dependence of (0,0,2) peak intensity between 5–150 K. (c) The (1,1,1) reflection shows an enhancement below T_C, but exhibits no anomaly across $T^* \approx 60$ K. The solid lines are guides to the eye.

and isotropic itinerant ferromagnetic $SrRuO_3$. The existence of spin fluctuation and competing magnetic order is evident from the linear-T behavior and negative magnetoresistence of the inplane resistivity ρ_{ab} [13]. Neutron diffraction studies confirmed the presence of a complex evolution of the spin configuration at zero field [17,18,25]. Capogna *et al.* analyzed the intensities of various magnetic reflections and proposed a layer-dependent antiferromagnetism competing with the ferromagnetic order in the intermediate temperature range [18]. Upon cooling, only the Ru ions of the central-layer octahedra have a persisting c-axis spin component, while the Ru ions at the two outer layers tend to align their moments in the basal plane forming antiferromagnetic correlations. The effect is most pronounced at T^* and reverts to the collinear c-axis ferromagnetic order upon further cooling, highlighting the competition between FM and AFM coupling and the importance of the layer-dependent magnetic anisotropy. However, this complex change in magnetic structure evolution is not observed in the Ir-doped $Sr_4Ru_3O_{10}$. Comparing the neutron diffraction data collected at 5 K with those at 150 K, there is no additional superstructure or forbidden peaks of the high temperature phase, ruling out the formation of an antiferromagnetic order or a structural phase transition. In previous neutron diffraction studies, notable temperature variations were observed in Bragg reflections $(0, 0, 2n)$ of the undoped $Sr_4Ru_3O_{10}$ [17,18]. Since the coherent magnetic scattering intensity probes the spin component $\mathbf{S}_\perp$ perpendicular to the momentum transfer $\mathbf{Q}$, that is, $\mathbf{S}_\perp = \hat{\mathbf{Q}} \times (\mathbf{S} \times \hat{\mathbf{Q}})$; any additional increase in intensity at the allowed nuclear Bragg peak $(0, 0, 2n)$ would indicate a magnetic contribution from the in-plane spin component. Figure 3(b) shows the thermal evolution of the (0,0,2) peak intensity in zero field. It remains featureless across the entire temperature range of 5–150 K. This result contrasts with the broad hump appearing below the magnetic transition in pure $Sr_4Ru_3O_{10}$. On the other hand, the (1,1,1) reflection shows an increase in intensity below $T_C \approx 105$ K but no anomalous behavior near T^*. Together, the neutron diffraction results reveal a conventional second order phase transition without complex evolution of spin configuration.

The crystal structure determined allows an accurate characterization of the magnetic configuration. Two Ru sites (4*a* and 8*b*) are located at (0,0,0) and (0,0,0.14) Wyckoff positions. One of the eight maximal magnetic space groups, $Bb'e'm$ (No. 64.475, Belov-Neronova-Smirnova setting [26]), corresponds to a collinear ferromagnetic spin order and adequately describes the collected intensities. Table I compares the calculated and measured intensities at 5 K with data at 150 K subtracted as background. All reflections at $(0, 0, l = 2n)$ have negligible intensity reaffirming the c-axis aligned spin direction, while the statistically significant reflections

TABLE I. Comparison of measured and refined magnetic Bragg peak intensities at zero field and $\mu_0 H = 4.5$ T. A twin domain population ratio of 49:51 is obtained from structural refinement. Magnetic form factor uses Ru^{1+} ion. Magnetic structure factors F^2 in units of fm^2.

q	F^2_{calc}(0 T)	F^2_{obs}(0 T)	F^2_{calc}(4.5 T)	F^2_{obs}(4.5 T)
(0 0 2)	0	−4(4)	62	63(3)
(0 0 4)	0	1(6)	59	55(6)
(0 0 6)	0	−9(21)	359	324(19)
(0 0 8)	0	28(15)	347	325(15)
(1 1 1)	328	331(10)	338	364(11)
(1 1 3)	20	12(6)	23	14(6)
(1 1 7)	159	138(23)	302	292(25)
(1 1 9)	8	57(11)	20	58(12)

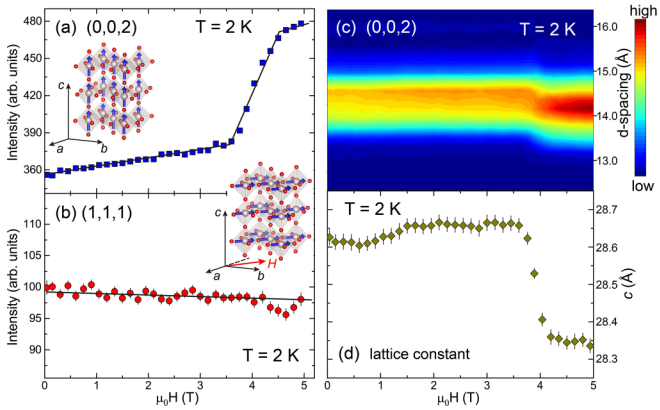

FIG. 4. (a) The field dependence of the (0,0,2) intensity increases abruptly above 3.7 T and levels off at 4.5 T. (b) The integrated intensity of the (1,1,1) Bragg peak is nearly field independent. Solid lines are guides to the eye. The insets illustrate the magnetic structures in zero field (left) and the in-plane field along the $[\bar{1}, 1, 0]$ direction (right) of Ir-doped $Sr_4Ru_3O_{10}$. (c) The contour plot shows the field dependence of the (0,0,2) reflection at 2 K. (d) The c-axis lattice parameter shows a sudden collapse around 3.7 T.

at $(1, 1, l)$ show modulated intensities due to the triple-layer phase factor. The refinement shows two Ru sites at the center and outer layers have moments of 1.14(2) and 1.04(3) μ_B/Ru, respectively. They are in accordance with the saturated moment shown in Fig. 1(c), a half size of 2 μ_B/Ru expected for an $S = 1$ system. The difference in moment size between the two sites is smaller compared to that of the pure $Sr_4Ru_3O_{10}$ where the ordered moments are 1.59(4) and 0.92(3) μ_B/Ru [16]. This is probably due to the reduced difference in bond distances between the Ru and apical oxygen atoms of the central- and outer-layer RuO_6 octahedra [24].

The flat thermal evolution of the (0,0,2) peak and the monotonic increase in (1,1,1) peak below T_C are in sharp contrast with the undoped $Sr_4Ru_3O_{10}$ and indicates the stabilization of the c-axis oriented spin order upon Ir doping. Such robust c-axis FM order is further manifested by a large increase in the critical field H_C driving the basal-plane metamagnetic transition. Figures 4(a) and 4(b) plot the same reflections monitoring the spin configuration upon application of magnetic fields along the $[-1, 1, 0]$ direction. The (0,0,2) peak shows a slow increase at low field but an abrupt enhancement above 3.7 T that completes at 4.5 T. In contrast, the (1,1,1) essentially shows no variation in intensity over the whole field range. Based on the integrated peak intensities listed in Table I, the magnetic structure is refined as a collinear spin order with moments completely aligned along the field direction within the basal plane. The c-axis lattice parameter collapses at the transition when the moments are in the basal plane [Fig. 4(c)]. This is in accordance with the negative thermal expansion of the c axis in the pure $Sr_4Ru_3O_{10}$ when it reenters the collinear FM state below T^* [16,27]. Such a strong magnetoelastic effect emphasizes an important role of orbital degrees of freedom, which is revealed by a Raman scattering study [14,28].

Several scenarios could explain the stabilization of the ferromagnetic order in the Ir-doped $Sr_4Ru_3O_{10}$. One possibility is the enhanced RuO_6 octahedral rotation in the triple-layer ruthenate. Our results bear some similarity with the distortion-induced ferromagnetism reported in the pure Sr_2RuO_4. Although it has an undistorted tetragonal structure [29] and dominant magnetic fluctuations at the incommensurate vector (0.33, 0.33, 0) [30], ferromagnetism was reported at the surface of the bulk crystal Sr_2RuO_4 [31], which is attributed to a soft-phonon mode that freezes into a static in-plane rotation of the RuO_6 [32]. The octahedral rotation reduces d-d electron hopping and leads to band narrowing, which increases the densities of states (DOS) at the Fermi energy and ultimately stabilizes the FM order [31]. A similar argument might be valid for the Ir-doped $Sr_4Ru_3O_{10}$. On the other hand, one should also consider the role of enhanced spin-orbit coupling (SOC) associated with 5d iridium ions, where the SOC strength λ increases strongly with the atomic number Z from 0.16 eV for 4d ruthenates to 0.4 eV for 5d iridates [33,34]. Substituting a considerable amount of iridium atoms at the Ru site effectively promotes the magnetic anisotropy [25]. It competes vigorously with Coulomb interaction U, filling of the density of states $g(E_f)$ at the Fermi surface, and eventually leads to a collinear spin order with c axis moment. The observed behavior is similar to the situation of weak ferromagnetic order along the c axis in the doped $Ca_2Ru_{1-x}Ir_xO_4$ [35].

The system resides near the borderline of magnetic stability as evidenced by the in-plane-field metamagnetic transition. Angle-resolved photoemission spectroscopy (ARPES) revealed flat bands a few tens of meVs below the Fermi surface [36]. The existence of a saddle-point-like feature with high DOS is closely related to van Hove singularities (vHS). They render a magnetic instability such that application of a small field shifts the vHS across the Fermi level E_F. One key difference between the triple-layer and other RP-series ruthenates is the role of t_{2g} orbitals. In the two-dimensional Sr_2RuO_4, the d_{xy} orbital is primarily responsible for the vHS at the zone boundary [37–39] and the resulting FM fluctuation [40–42]. However, the d_{xz}/d_{yz} orbitals are more relevant for the electronic properties in the triple-layer $Sr_4Ru_3O_{10}$. The hopping between neighboring Ru-O planes within the triple-layer split the electronic bands of 4d orbitals into bonding (B), nonbonding (NB), and antibonding (AB) d_{xz}/d_{yz} characters. The NB orbital has an odd symmetry and is not sensitive to the central layer, while the B and AB orbitals have even symmetry and contains dominant information of the central layer [43,44]. Future spin polarized ARPES studies would be helpful to investigate whether the layer-specific contribution can be resolved in the pure and Ir-doped $Sr_4Ru_3O_{10}$, thus providing an important constraint to understand the effect of electron correlation as well as the metamagnetic transition facilitated by spin-orbit coupling.

Materials with a metamagnetic transition are intriguing candidates for modern spintronics devices. The triple-layer $Sr_4Ru_3O_{10}$ is considered as a paradigmatic 4d transition metal oxide; the competing magnetic ground states and the low-field metamagnetic transition are caused by the delicate interplay of essential interactions of magnetic anisotropy, spin-orbit coupling, and electron correlation. The ability to achieve a giant response through small stimuli make it promising material for realizing low power consumption memories and computation

[45]. We have demonstrated that a small amount of iridium doping at the ruthenium site enhances the lattice distortion and stabilizes a magnetic order with perpendicular magnetization, a state actively pursued for swift and efficient switching, for example, in other topological antiferomagnets [46,47].

Research at ORNL's SNS was sponsored by the Scientific User Facilities Division, Office of Basic Energy Sciences, U.S. Department of Energy (DOE). Work at the University of Colorado was supported by NSF via Grant No. DMR 2204811.

[1] Y. Maeno, H. Hashimoto, K. Yoshida, S. Nishizaki, T. Fujita, J. G. Bednorz, and F. Lichtenberg, Superconductivity in a layered perovskite without copper, Nature (London) **372**, 532 (1994).

[2] G. M. Luke, Y. Fudamoto, K. M. Kojima, M. I. Larkin, J. Merrin, B. Nachumi, Y. J. Uemura, Y. Maeno, Z. Q. Mao, Y. Mori, H. Nakamura, and M. Sigrist, Time-reversal symmetry-breaking superconductivity in Sr_2RuO_4, Nature (London) **394**, 558 (1998).

[3] S. Benhabib, C. Lupien, I. Paul, L. Berges, M. Dion, M. Nardone, A. Zitouni, Z. Q. Mao, Y. Maeno, A. Georges, L. Taillefer, and C. Proust, Ultrasound evidence for a two-component superconducting order parameter in Sr_2RuO_4, Nat. Phys. **17**, 194 (2021).

[4] S. Ghosh, A. Shekhter, F. Jerzembeck, N. Kikugawa, D. A. Sokolov, M. Brando, A. P. Mackenzie, C. W. Hicks, and B. J. Ramshaw, Thermodynamic evidence for a two-component superconducting order parameter in Sr_2RuO_4, Nat. Phys. **17**, 199 (2021).

[5] S. A. Grigera, R. S. Perry, A. J. Schofield, M. Chiao, S. R. Julian, G. G. Lonzarich, S. I. Ikeda, Y. Maeno, A. J. Millis, and A. P. Mackenzie, Magnetic Field-Tuned Quantum Criticality in the Metallic Ruthenate $Sr_3Ru_2O_7$, Science **294**, 329 (2001).

[6] R. S. Perry, L. M. Galvin, S. A. Grigera, L. Capogna, A. J. Schofield, A. P. Mackenzie, M. Chiao, S. R. Julian, S. I. Ikeda, S. Nakatsuji, Y. Maeno, and C. Pfleiderer, Metamagnetism and Critical Fluctuations in High Quality Single Crystals of the Bilayer Ruthenate $Sr_3Ru_2O_7$, Phys. Rev. Lett. **86**, 2661 (2001).

[7] A. Callaghan, C. W. Moeller, and R. Ward, Magnetic interactions in ternary ruthenium oxides, Inorg. Chem. **5**, 1572 (1966).

[8] G. Cao, S. McCall, M. Shepard, J. E. Crow, and R. P. Guertin, Thermal, magnetic, and transport properties of single-crystal $Sr_{1-x}Ca_xRuO_3$ ($0 \leqslant x \leqslant 1.0$), Phys. Rev. B **56**, 321 (1997).

[9] G. Koster, L. Klein, W. Siemons, G. Rijnders, J. S. Dodge, C.-B. Eom, D. H. A. Blank, and M. R. Beasley, Structure, physical properties, and applications of $SrRuO_3$ thin films, Rev. Mod. Phys. **84**, 253 (2012).

[10] H. Zheng, W. H. Song, J. Terzic, H. D. Zhao, Y. Zhang, Y. F. Ni, L. E. DeLong, P. Schlottmann, and G. Cao, Observation of a pressure-induced transition from interlayer ferromagnetism to intralayer antiferromagnetism in $Sr_4Ru_3O_{10}$, Phys. Rev. B **98**, 064418 (2018).

[11] G. Cao and L. DeLong, *Chapter 4, Physics of Spin-Orbit-Coupled Oxides* (Oxford Univ. Press, Oxford, United Kingdom, 2021).

[12] M. K. Crawford, R. L. Harlow, W. Marshall, Z. Li, G. Cao, R. L. Lindstrom, Q. Huang, and J. W. Lynn, Structure and magnetism of single crystal $Sr_4Ru_3O_{10}$: A ferromagnetic triple-layer ruthenate, Phys. Rev. B **65**, 214412 (2002).

[13] G. Cao, L. Balicas, W. H. Song, Y. P. Sun, Y. Xin, V. A. Bondarenko, J. W. Brill, S. Parkin, and X. N. Lin, Competing ground states in triple-layered $Sr_4Ru_3O_{10}$: Verging on itinerant ferromagnetism with critical fluctuations, Phys. Rev. B **68**, 174409 (2003).

[14] R. Gupta, M. Kim, H. Barath, S. L. Cooper, and G. Cao, Field- and pressure-induced phases in $Sr_4Ru_3O_{10}$: A spectroscopic investigation, Phys. Rev. Lett. **96**, 067004 (2006).

[15] W. Bao, Z. Q. Mao, M. Zhou, J. Hooper, J. W. Lynn, R. S. Freitas, P. Schiffer, Y. Liu, H. Q. Yuan, and M. Salamon, Magnetic transition and magnetic structure of $Sr_4Ru_3O_{10}$, arXiv:cond-mat/0607428.

[16] V. Granata, L. Capogna, M. Reehuis, R. Fittipaldi, B. Ouladdiaf, S. Pace, M. Cuoco, and A. Vecchione, Neutron diffraction study of triple-layered $Sr_4Ru_3O_{10}$, J. Phys.: Condens. Matter **25**, 056004 (2013).

[17] M. Zhu, P. G. Li, Y. Wang, H. B. Cao, W. Tian, H. D. Zhang, B. D. Phelan, Z. Q. Mao, and X. Ke, Temperature- and field-driven spin reorientations in triple-layer ruthenate $Sr_4Ru_3O_{10}$, Sci. Rep. **8**, 3914 (2018).

[18] L. Capogna, V. Granata, B. Ouladdiaf, J. Rodriguez-Velamazan, R. Fittipaldi, and A. Vecchione, Layer dependent antiferromagnetism in the $Sr_4Ru_3O_{10}$ ruthenate at the metamagnetic-like transition, J. Magn. Magn. Mater. **493**, 165698 (2020).

[19] S. Chikara, V. Durairaj, W. H. Song, Y. P. Sun, X. N. Lin, A. Douglass, G. Cao, P. Schlottmann, and S. Parkin, Borderline magnetism in $Sr_4Ru_3O_{10}$: Impact of La and Ca doping on itinerant ferromagnetism and metamagnetism, Phys. Rev. B **73**, 224420 (2006).

[20] F. Ye, Y. Liu, R. Whitfield, R. Osborn, and S. Rosenkranz, Implementation of cross correlation for energy discrimination on the time-of-flight spectrometer CORELLI, J. Appl. Crystallogr. **51**, 315 (2018).

[21] A. Damascelli, D. H. Lu, K. M. Shen, N. P. Armitage, F. Ronning, D. L. Feng, C. Kim, Z.-X. Shen, T. Kimura, Y. Tokura, Z. Q. Mao, and Y. Maeno, Fermi Surface surface states, and surface reconstruction in Sr_2RuO_4, Phys. Rev. Lett. **85**, 5194 (2000).

[22] D. J. Singh and I. I. Mazin, Electronic structure and magnetism of $Sr_3Ru_2O_7$, Phys. Rev. B **63**, 165101 (2001).

[23] A. Tamai, M. P. Allan, J. F. Mercure, W. Meevasana, R. Dunkel, D. H. Lu, R. S. Perry, A. P. Mackenzie, D. J. Singh, Z.-X. Shen, and F. Baumberger, Fermi surface and van hove singularities in the itinerant metamagnet $Sr_3Ru_2O_7$, Phys. Rev. Lett. **101**, 026407 (2008).

[24] See Supplemental Material at http://link.aps.org/supplemental/10.1103/PhysRevB.108.L241109 for further details of space group determination, structural refinement, and magnetic structure analysis, which includes [12,48–53].

[25] V. Granata, L. Capogna, F. Forte, M.-B. Lepetit, R. Fittipaldi, A. Stunault, M. Cuoco, and A. Vecchione, Spin-orbital nature of the high-field magnetic state in the $Sr_4Ru_3O_{10}$, Phys. Rev. B **93**, 115128 (2016).

[26] N. V. Belov, N. N. Neronova, and T. S. Smirnova, Shubnikov groups, Kristallografiya **2**, 315 (1957).

[27] F. Weickert, L. Civale, B. Maiorov, M. Jaime, M. B. Salamon, E. Carleschi, A. M. Strydom, R. Fittipaldi, V. Granata, and A. Vecchione, Missing magnetism in $Sr_4Ru_3O_{10}$: Indication for Antisymmetric Exchange Interaction, Sci. Rep. **7**, 3867 (2017).

[28] M. N. Iliev, V. N. Popov, A. P. Litvinchuk, M. V. Abrashev, J. Bäckström, Y. Y. Sun, R. L. Meng, and C. W. Chu, Comparative Raman studies of Sr_2RuO_4, $Sr_3Ru_2O_7$ and $Sr_4Ru_3O_{10}$, Phys. B: Condens. Matter **358**, 138 (2005).

[29] T. Vogt and D. J. Buttrey, Low-temperature structural behavior of Sr_2RuO_4, Phys. Rev. B **52**, R9843 (1995).

[30] M. Braden, Y. Sidis, P. Bourges, P. Pfeuty, J. Kulda, Z. Mao, and Y. Maeno, Inelastic neutron scattering study of magnetic excitations in Sr_2RuO_4, Phys. Rev. B **66**, 064522 (2002).

[31] R. Matzdorf, Z. Fang, Ismail, J. Zhang, T. Kimura, Y. Tokura, K. Terakura, and E. W. Plummer, Ferromagnetism stabilized by lattice distortion at the surface of the p-Wave superconductor Sr_2RuO_4, Science **289**, 746 (2000).

[32] M. Braden, G. André, S. Nakatsuji, and Y. Maeno, Crystal and magnetic structure of Ca_2RuO_4: Magnetoelastic coupling and the metal-insulator transition, Phys. Rev. B **58**, 847 (1998).

[33] G. Cao and L. DeLong, *Frontiers of 4d- and 5d- Transition Metal Oxides* (World Scientific Publishing, Singapore, 2013).

[34] D. I. Khomskii, *Chapter 2, Transition Metal Compounds* (Cambridge Univ. Press, Cambridge, United Kingdom, 2014).

[35] S. J. Yuan, J. Terzic, J. C. Wang, L. Li, S. Aswartham, W. H. Song, F. Ye, and G. Cao, Evolution of magnetism in single-crystal $Ca_2Ru_{1-x}Ir_xO_4$ ($0 \leqslant x \leqslant 0.65$), Phys. Rev. B **92**, 024425 (2015).

[36] P. Ngabonziza, E. Carleschi, V. Zabolotnyy, A. Taleb-Ibrahimi, F. Bertran, R. Fittipaldi, V. Granata, M. Cuoco, A. Vecchione, and B. P. Doyle, Fermi surface and kink structures in $Sr_4Ru_3O_{10}$ revealed by synchrotron-based ARPES, Sci. Rep. **10**, 21062 (2020).

[37] T. Oguchi, Electronic band structure of the superconductor Sr_2RuO_4, Phys. Rev. B **51**, 1385 (1995).

[38] D. J. Singh, Relationship of Sr_2RuO_4 to the superconducting layered cuprates, Phys. Rev. B **52**, 1358 (1995).

[39] A. P. Mackenzie, S. R. Julian, A. J. Diver, G. J. McMullan, M. P. Ray, G. G. Lonzarich, Y. Maeno, S. Nishizaki, and T. Fujita, Quantum oscillations in the layered perovskite superconductor Sr_2RuO_4, Phys. Rev. Lett. **76**, 3786 (1996).

[40] D. F. Agterberg, T. M. Rice, and M. Sigrist, Orbital dependent superconductivity in Sr_2RuO_4, Phys. Rev. Lett. **78**, 3374 (1997).

[41] T. Imai, A. W. Hunt, K. R. Thurber, and F. C. Chou, ^{17}O NMR evidence for orbital dependent ferromagnetic correlations in Sr_2RuO_4, Phys. Rev. Lett. **81**, 3006 (1998).

[42] I. I. Mazin and D. J. Singh, Competitions in layered ruthenates: Ferromagnetism versus antiferromagnetism and triplet versus singlet pairing, Phys. Rev. Lett. **82**, 4324 (1999).

[43] G. Gebreyesus, P. Ngabonziza, J. Nagura, N. Seriani, O. Akin-Ojo, and R. M. Martin, Electronic structure and magnetism of the triple-layered ruthenate $Sr_4Ru_3O_{10}$, Phys. Rev. B **105**, 165119 (2022).

[44] P. Ngabonziza, J. D. Denlinger, A. V. Fedorov, G. Cao, J. W. Allen, G. Gebreyesus, and R. M. Martin, Spin-resolved electronic structure of ferromagnetic triple-layered ruthenate $Sr_4Ru_3O_{10}$, arXiv:2305.07222.

[45] Y. Liu, W. Chu, J. Yang, G. Liu, H. Du, W. Ning, L. Ling, W. Tong, Z. Qu, G. Cao, Z. Xu, and M. Tian, Magnetic reversal in $Sr_4Ru_3O_{10}$ nanosheets probed by anisotropic magnetoresistance, Phys. Rev. B **98**, 024425 (2018).

[46] K. Kondou, H. Chen, T. Tomita, M. Ikhlas, T. Higo, A. H. MacDonald, S. Nakatsuji, and Y. Otani, Giant field-like torque by the out-of-plane magnetic spin Hall effect in a topological antiferromagnet, Nat. Commun. **12**, 6491 (2021).

[47] T. Higo, K. Kondou, T. Nomoto, M. Shiga, S. Sakamoto, X. Chen, D. Nishio-Hamane, R. Arita, Y. Otani, S. Miwa, and S. Nakatsuji, Perpendicular full switching of chiral antiferromagnetic order by current, Nature (London) **607**, 474 (2022).

[48] M. I. Aroyo, editor, *International Tables for Crystallography: Space-Group Symmetry*, 2nd ed., International Tables for Crystallography Vol. A (International Union of Crystallography, Chester, England, 2016).

[49] V. F. Sears, Neutron scattering lengths and cross sections, Neutron News **3**, 26 (1992).

[50] V. Petříček, L. Palatinus, J. Plášil, and M. Dušek, Jana2020 – a new version of the crystallographic computing system Jana, Z. Kristallogr. - Cryst. Mater. **238**, 271 (2023).

[51] P. J. Becker and P. Coppens, Extinction within the limit of validity of the Darwin transfer equations. II. Refinement of extinction in spherical crystals of SrF_2 and LiF, Acta Cryst. A **30**, 148 (1974).

[52] S. Parsons, Introduction to twinning, Acta Crystallogr. D **59**, 1995 (2003).

[53] E. Prince, H. Fuess, T. Hahn, H. Wondratschek, U. Müller, U. Shmueli, E. Prince, A. Authier, V. Kopský, D. B. Litvin, M. G. Rossmann, E. Arnold, S. Hall, and B. McMahon, editors, *International Tables for Crystallography: Mathematical, Physical and Chemical Tables*, 1st ed., International Tables for Crystallography Vol. C (International Union of Crystallography, Chester, England, 2006).